

pubs.acs.org/joc Article

# Design, Synthesis, and Physicochemical Studies of Configurationally Stable $\beta$ -Carboline Atropisomers

Kristen M. Baker, Colby J. Agostino, Emily A. Orloff, Lorenzo D. Battistoni, Riley R. Hughes, Erin M. McHugh, Michael P. Shaw, Jordan Nafie, and Seann P. Mulcahy\*



Cite This: https://doi.org/10.1021/acs.joc.2c01675



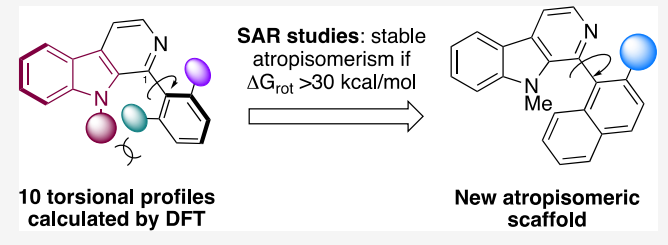
**ACCESS** I

III Metrics & More

Article Recommendations

s Supporting Information

**ABSTRACT:** Axially chiral atropisomers have energetic barriers to rotation,  $\Delta G_{\rm rov}$  that prevent racemization of the respective enantiomers. We used computational modeling to develop a suite of 10 bio-inspired 1-aryl- $\beta$ -carbolines with varying  $\Delta G_{\rm rov}$  from which a strong structure—activity relationship was observed for 2-substituted-1-naphthyl substituents. We then synthesized two of these atropisomers, 1d and 1f, by a four-step racemic synthesis and resolved the enantiomers via chiral chromatography. Racemization studies revealed experimental  $\Delta G_{\rm rot}$  values of 39.5



and 33.0 kcal/mol for 1d and 1f, respectively, which were consistent with our computational results. These atropisomers exhibited long half-lives, which allowed for their physicochemical characterization and stereochemical assignment via UV—vis spectroscopy, fluorescence spectroscopy, electronic circular dichroism, and vibrational circular dichroism.

#### INTRODUCTION

Axial chirality is an important source of stereochemical handedness in small molecules that occurs when a defined, nonsuperimposable arrangement of atoms or groups exists about a central axis. 1-3 Small molecules such as allenes, spiranes, helicenes, and atropisomers are all axially chiral and constitute a wide range of spatially diverse molecules with important spectral, photophysical, and biological properties. Unique to this group, atropisomers form when molecules have a  $\sigma$  bond that cannot undergo full rotation, usually due to a steric or electronic effect (Figure 1a). When appropriately substituted, atropisomers can become enantiomeric, but their configurational stability is time-dependent. The magnitude of the barrier to rotation  $(\Delta G_{rot})$  determines the rate of racemization, with half-lives ranging from seconds to millennia.<sup>4</sup> Because of this, configurationally stable atropisomers are a privileged scaffold for organic chemists.5 For example, chiral atropisomeric ligands enjoy a rich history in asymmetric catalysis,6 and many natural products contain an atropisomeric axis.7 Chiral atropisomers are further found in molecular devices, molecular machines, and luminescent sensors.8 Finally, harnessing restricted bond rotation has become a common tool in drug discovery in the quest for more potent and selective small molecules.9

Typical biaryl atropisomerism exploits the geometrical constraints inherent to a biaryl axis containing two sixmembered aromatic rings with several *ortho* substituents. Substituting an all-carbon aromatic ring for a pyridine or isoquinoline heterocycle would make the isolation of stable atropisomers much more challenging (Figure 1b). Replacing

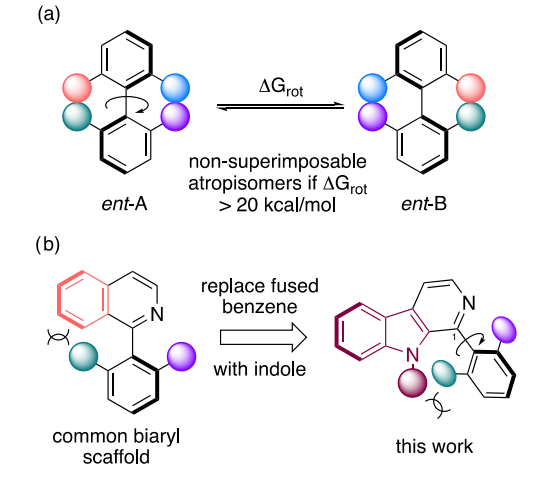


**Figure 1.** (a) Atropisomerism as a unique source of axial chirality, (b) our design of atropisomeric 1-aryl-β-carbolines.

carbon with nitrogen removes the possibility of *ortho*-substitution and would decrease the barrier to rotation substantially. For example, the common asymmetric ligand BINOL has a barrier to rotation of 37.8 kcal/mol, which is

Received: July 15, 2022

configurationally stable  $(t_{1/2}=1.7\times 10^7 \text{ years}).^{4\text{b},10}$  By contrast, replacing one of the naphthol rings in BINOL with an isoquinoline ring to produce 1-(1'-isoquinolyl)-naphthol reduces the barrier to rotation to 26.4 kcal/mol and results in more rapid racemization  $(t_{1/2}=690 \text{ h}).^{11}$  Thus, harnessing atropisomerism in nitrogen-containing heterocycles is a unique challenge for synthetic chemists.

Several research groups have developed elegant catalytic asymmetric strategies toward a wide range of heteroaromatic atropisomeric scaffolds, including pyridyl systems. 5c,12 Techniques for the preparation of atropisomers containing a 2-pyridyl or 1-isoquinolyl functional group have been incredibly impactful but have relied heavily on the isoquinolyl system to restrict rotation. 13 Our approach has been to use the  $\beta$ carboline scaffold, which has a fused pyrido [3,4-b] indole ring system with potential for atropisomerism if arylation occurs at the 1-position of the core scaffold. While the pyridoindole skeleton is a 5,6-ring framework that nominally decreases steric encumbrance near the atropisomeric axis, we sought to functionalize the indole ring via alkylation to insert steric bulk closer to the axis of interest. Such a functionalization is only available in this privileged heterocycle. Combined with our long-standing interest in the chemical biology of the  $\beta$ carboline natural products, we hypothesized that atropisomerism could be introduced into the  $\beta$ -carboline scaffold with high barriers to rotation, thus giving us entry into a new area of molecular space.

 $\beta$ -Carbolines that contain aryl groups at the 1-position of the core scaffold are incredibly rare in nature. <sup>14</sup> Of the hundreds of  $\beta$ -carboline-containing natural products, only a few contain different aryl or heteroaryl functionality at the 1-position, including eudistomins A, M, and U, nitraridine and nitramarine, and chaetogline F (Figure 2). <sup>15</sup> However, it is

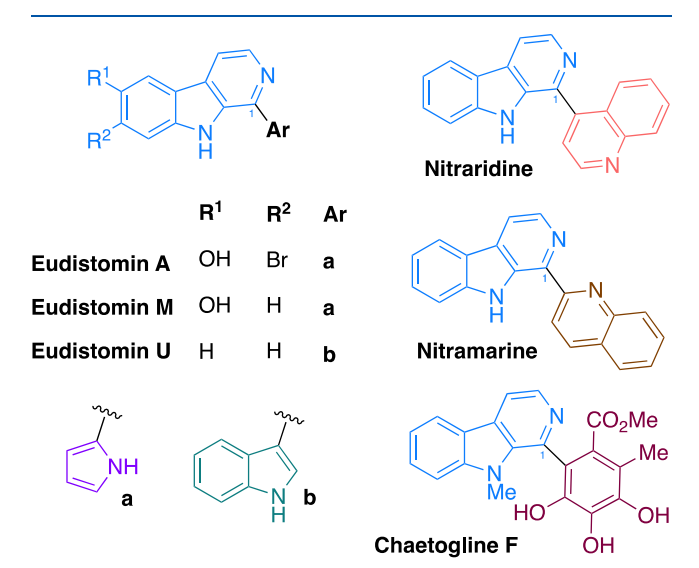


**Figure 2.** β-Carboline natural products containing 1-aryl or 1-heteroaryl groups.

unclear what role these groups play in their observed biological activity. We have shown that eudistomin U has weak unspecific binding to DNA, but no detailed studies of this substitution pattern and its effect on bioactivity have been performed. This is striking since one of the unique features of 1-aryl- $\beta$ -carbolines is their potential for atropisomerism. For example, in eudistomin U and chaetogline F, the  $\beta$ -carboline scaffold

and appended aryl ring can only lie coplanar in a high energy transition state. This leads to a sizable barrier for rotation around the biaryl axis and can result in atropisomeric (or proatropisomeric) binding to a biological target. Indeed, many groups have shown that atropspecific binding to macromolecular targets can be a useful design tool in chemical biology and drug discovery. However, isolating the individual enantiomers of axially chiral  $\beta$ -carbolines has never been achieved. We report herein the discovery of a new class of atropisomers based on the  $\beta$ -carboline scaffold that exhibit remarkable configurational stability. We combine computational modeling with synthetic and physicochemical studies to demonstrate that atropisomeric  $\beta$ -carbolines are stable species worthy of continued study.

#### ■ RESULTS AND DISCUSSION

pubs.acs.org/joc

We began our study by designing a small library of 1-aryl-βcarbolines and using density functional theory (DFT) to determine which functional groups gave high barriers to rotation. As guidance, we relied on the work of LaPlante and co-workers, who set a standard of 30 kcal/mol as the minimum barrier for the development of atropisomeric drug candidates as single enantiomers. 9b-d Since we suspected that rapid isomerization would occur with an unsubstituted indole N-H, our initial work was performed with a methyl group on the indole nitrogen to increase steric bulk around the Caryl-Caryl bond. Using Gaussian 16, we assembled ten different molecules with aromatic rings at the 1-position of the  $\beta$ carboline. Compound 1a was used as a reference compound since it was unable to exhibit atropisomerism. Compounds 1b-1j contained either substituent groups at the ortho position, a fused ring, or both (Figure 3).

To determine the barrier to rotation of these molecules computationally, we calculated the geometry-optimized equilibrium free energy and then determined the two transition states that arose upon rotation about the  $C_{aryl}$ - $C_{aryl}$  bond. The difference between the free energy of the lowest transition state and the equilibrium free energy gave us the calculated barriers to rotation ( $\Delta G_{\text{rot}}$ ) shown in Figure 3. The  $\Delta G_{\text{rot}}$  of the monoortho-phenyl- (1b) and naphthyl-substituted (1c) compounds were higher relative to reference compound 1a. However, additional steric bulk would still be needed to access stable atropisomers. While many 2,6-disubstituted phenyl rings could be imagined that have sufficient steric bulk, we chose to focus on the naphthyl series due to its rigidity and ease with which the 2-position could be modified computationally to provide useful structure-activity data. As expected, the remaining compounds 1d-1j each gave high calculated  $\Delta G_{rot}$ , consistent with configurationally stable atropisomerism. In most cases, the lower energy transition state occurred when the substituent group at the 2-position was syn to the methyl group on the indole. The exceptions were compound 1d, in which the tetrahedral methyl groups occlude each other, compound 1e, in which the two transition states were about equal, compound 1j, which has an sp<sup>2</sup>-hybridized atom, and compound 1g, in which an intramolecular hydrogen bond is observed. The two highest calculated  $\Delta G_{\rm rot}$  values were observed for 1d and 1e, which have methyl and chloro groups that are known to have large steric interference values in biaryl systems. 18 By contrast, the 2-methoxy (1f) and 2-hydroxy (1g) derivatives were closer to 30 kcal/mol, which is consistent with smaller effective radii for these groups. The analogous nitrogen derivatives 1h and 1i each gave calculated  $\Delta G_{\rm rot}$  values higher than 1f and 1g, which

Me

AG = 12.6 
$$\Delta G$$
 = 19.6  $\Delta G$  = 19.8  $\Delta G$  = 39.1  $\Delta G$  = 40.2

f

g

h

i

j

 $\Delta G$  = 32.1  $\Delta G$  = 30.7  $\Delta G$  = 36.7  $\Delta G$  = 33.9  $\Delta G$  = 36.5

**Figure 3.** Calculated barrier to rotation ( $\Delta G_{\text{rot}}$  kcal/mol) of 1-aryl- $\beta$ -carbolines.

can be explained by a combination of larger steric interference and effective radii values compared to their oxygen-containing isosteres. The presence of a 2-nitro group (1j), which is similar in size to a dimethylamino group, did not impact the barrier to rotation despite the change in hybridization at the nitrogen atom.

With strong evidence that 2-naphthyl substituents were the best candidates to induce atropisomerism experimentally, we embarked on the synthesis and resolution of two compounds in this series, 1d and 1f. These compounds were chosen as model atropisomers with  $\Delta G_{\rm rot}$  near or above 30 kcal/mol. The synthesis of these substrates was accomplished according to Scheme 1. Commercially available N-methylindole-2-carboxylic acid 2 was treated with aminoacetaldehyde dimethyl acetal 3 and carbonyldiimidazole to give the coupled amide product 4. Acid-promoted deprotection, cyclization, and dehydration of 4 was accomplished in neat TFA. This was

## Scheme 1. Synthesis of Racemic 1-Aryl-β-carboline Atropisomers via Suzuki Cross-Coupling

followed by direct conversion of the resulting pyridone to the triflate 5 in excellent yield. Triflate 5 was then subjected to Suzuki cross-coupling conditions with the appropriate boronic acid to give the racemic 1-aryl- $\beta$ -carbolines 1d and 1f in good yields.

To determine the experimental  $\Delta G_{\text{rot}}$  the enantiomers of 1d and 1f were separated by chiral HPLC, and a thermal

racemization kinetics study was performed. The individual enantiomers proved to be very stable at room temperature, so the racemization kinetics study was performed at elevated temperatures to give the experimental barriers to rotation and half-lives shown in Table 1 (see the Supporting Information for full experimental details). At a value of 39.5 kcal/mol, the experimental  $\Delta G_{\rm rot}$  for compound 1d is approaching the limits

Table 1. Experimental Barriers to Rotation of  $\beta$ -Carboline Atropisomers

Compound	Experimental $\Delta G_{rot}$	t <sub>1/2</sub> at 25 °C
N Me Me	39.5 kcal/mol	1.50 x 10 <sup>8</sup> years
N OMe Ne Me	33.0 kcal/mol	2.60 x 10 <sup>3</sup> years
N Me	29.5 kcal/mol	7.11 years

of detection for such species, confirming that it is configurationally inert ( $t_{1/2} = 1.5 \times 10^8$  years at room temperature). Very few experimentally determined barriers to rotation have been reported in the literature with such high configurational stability, but we should note that compound 1d has a  $\Delta G_{
m rot}$ that is 1.7 kcal/mol higher than the commonly used asymmetric ligand BINOL. 10a In addition, the experimental results in Table 1 are consistent with our computational data, which show that the presence of a methoxy group reduces the barrier to rotation compared to a methyl group on the naphthyl ring. Interestingly, when we prepared an analogue of 1d that did not have a methyl group on the indole nitrogen (compound 7), we measured an experimental barrier to rotation of 29.5 kcal/mol (calculated  $\Delta G_{\text{rot}} = 27.9 \text{ kcal/mol}$ ), consistent with slow racemization. This suggests that the development of configurationally stable molecules of this type does not require substitution on the indole nitrogen.

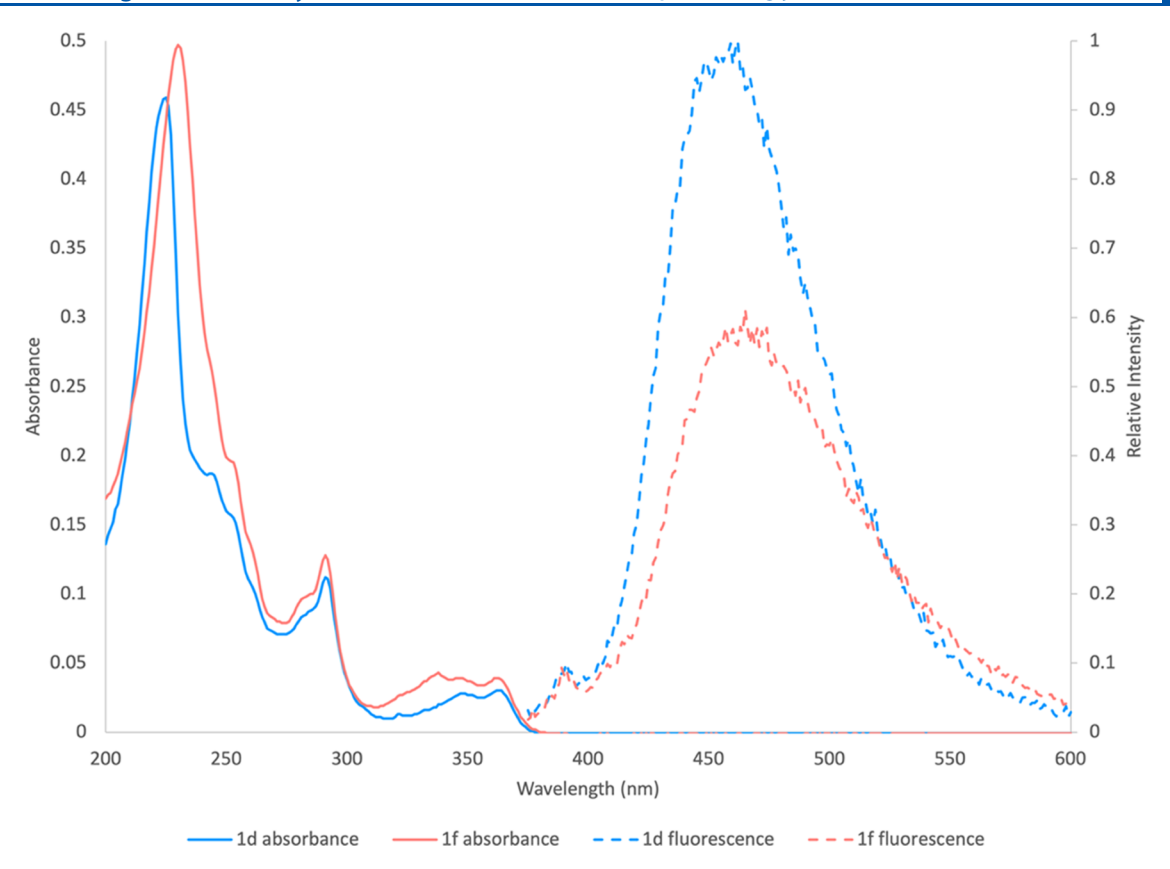


Figure 4. Electronic absorption spectra (solid lines, 10  $\mu$ M 1d and 1f in EtOH) and fluorescence emission spectra (dashed lines, 20  $\mu$ M 1d and 10  $\mu$ M 1f in EtOH,  $\lambda_{\rm ex}$  = 345 nm) of atropisomeric *β*-carbolines.

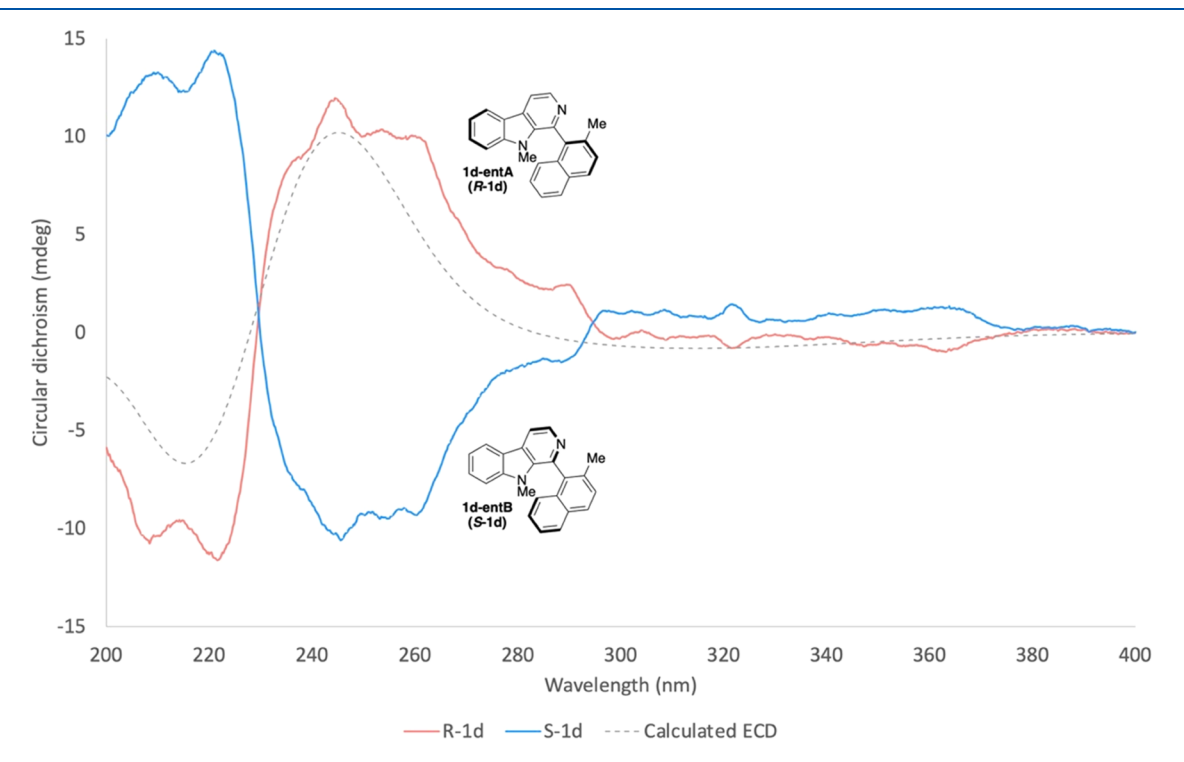


Figure 5. Calculated and experimental circular dichroism spectra of 200 µM 1d-entA (R-1d) and 1d-entB (S-1d) in EtOH.

 $\beta$ -Carbolines are known to have interesting photophysical properties, and we sought to characterize this behavior using compounds 1d and 1f. The electronic absorption and fluorescence emission spectra are shown in Figure 4. While

these compounds were only weakly fluorescent, a Stokes shift was observed for both 1d and 1f (117 and 120 nm, respectively). Low fluorescence quantum yields for 1d ( $\phi_F$  = 0.15) and 1f ( $\phi_F$  = 0.09) were observed relative to the known



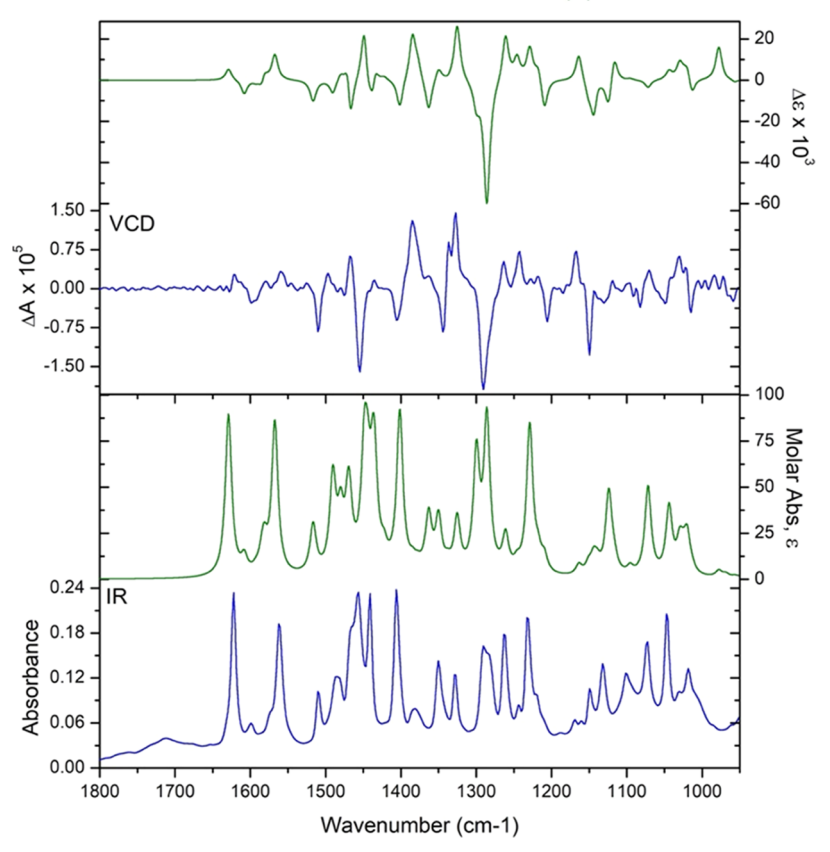


Figure 6. Comparison of the experimental and DFT-calculated IR and VCD spectra for 1d-entA (R-1d).

 $\beta$ -carboline standard harmane ( $\phi_F = 0.83$ ), which is indicative of conformational flexibility in the system. <sup>22</sup>

Finally, we turned our attention to the way in which the individual enantiomers of 1d and 1f interacted with polarized light. The circular dichroism spectra for 1d-entA and 1d-entB, the first and second compounds that eluted from the chiral HPLC column, respectively, are shown in Figure 5. The typical mirrored pattern is observed for the pair of enantiomers, and the helicity of these compounds is consistent with other biaryl atropisomers, with the strongest signal observed at 222 and 245 nm. To determine the absolute configuration of these compounds, we calculated the electronic circular dichroism (ECD) spectrum of R-1d using Gaussian '09 (Wallingford, CT) and compared it to the experimental data shown in Figure 5.<sup>23</sup> From this, we were able to identify that **1d-entA** has the *R*configuration. The same analysis was performed for the enantiomers of 1f, which indicated that the first compound to elute from the chiral HPLC column (1f-entA) had the Sconfiguration (see Figure S7 in the Supporting Information). In both cases, the substituent group on the naphthyl ring is positioned above the plane of the  $\beta$ -carboline ring, as depicted in Figure 5.

Vibrational circular dichroism (VCD) was employed as a complementary method for confirming the absolute configurations of atropisomers 1d and 1f.<sup>24</sup> Despite the relatively small amounts of material available (~5 mg each), the spectra obtained were of excellent quality (Figure 6). Optimal signal-to-noise levels for VCD are achieved when IR absorbance is in the range of 0.2–0.8 Å for bands of interest. While the absorbances for these compounds were relatively low (0.24 and 0.32 Å max, respectively, for 1d and 1f), the VCD

intensities were nonetheless impressive, in line with previously published VCD of atropisomers.<sup>25</sup> In particular, compound 1f had a very intense couplet  $(1.5 \times 10^{-4} \text{ peak to peak})$  centered at 1260 cm<sup>-1</sup>, resulting from C-O-C asymmetric stretching coupled with aromatic ring stretching. These two compounds exist primarily in a single conformation, enabling multiple DFT methods to be run without a high cost of computing resources. Two different functionals (B3LYP and B3PW91) each were utilized with two basis sets (6-31G(d) and cc-pVTZ) in Gaussian '09 to produce four sets of theoretical IR and VCD spectra for each compound. Each calculation produced results that could be matched to the experimental spectra to assign the absolute configuration, with the combination of cc-pVTZ/ B3PW91 giving the closest agreement. These results were quantified using BioTools (Jupiter, FL) CompareVOA software, with high neighborhood similarity and ESI values for both compounds. 26 As expected, the VCD results aligned with those from ECD, thus confirming the absolute configurations as R for 1d-entA and S for 1f-entA.

#### CONCLUSIONS

In summary, we have described the computational design, experimental synthesis, stereochemical resolution, and absolute configuration determination of configurationally stable atropisomers containing the  $\beta$ -carboline scaffold. With a remarkably inert chiral axis (up to  $\Delta G_{\rm rot} = 39.5~{\rm kcal/mol}$ ), this skeleton has great potential in the synthesis of atropisomeric natural products, drug-like probe molecules, chiral ligands or organocatalysts, and functional materials. Much more work still needs to be done to fully harness this potential, including the development of catalytic asymmetric

methods toward these molecules. Given that this is the first time molecules of this type have been prepared enantiomerically pure, our calculations and associated experimental spectra give us confidence that we will be able to identify the absolute configuration of similar scaffolds in the future more rapidly.

#### EXPERIMENTAL SECTION

General Procedures. All reactions were performed in single-neck, oven-dried, round-bottomed flasks unless otherwise noted. Each reaction flask was fitted with a rubber septum under a positive pressure of nitrogen and charged with a magnetic stir bar. Air- and moisture-sensitive liquids were transferred via a syringe. For reactions that required heating, a mineral oil bath was heated to the appropriate temperature using a thermocouple. Organic solutions were concentrated by rotary evaporation at 30-33 °C. Automated flashcolumn chromatography was performed on a Biotage Isolera One using Biotage SNAP Ultra and Sfär cartridges prepacked with 25 mm Biosphere silica gel, Sfär, or KP-Sil silica gel. Analytical thin-layered chromatography (TLC) was performed using plastic plates precoated with silica gel (0.25 mm, 60 Å pore size) impregnated with a fluorescent indicator (254 nm). TLC plates were visualized by exposure to ultraviolet light (UV). Microwave-accelerated reactions were performed using sealed vessel, oven-dried, glass microwave tubes in a single-port Discover System (908005) from CEM Corporation set to a maximum power of 300 W and a maximum pressure of 280 psi. The reaction mixture temperature was monitored using the builtin calibrated infrared sensor.

**Materials.** Chromatography solvents were used as received from Greenfield Global. All other commercial reagents were used as received from Sigma-Aldrich. VCD experiments were performed in  $CDCl_3$  (w/silver foil) from Cambridge Isotope Labs and used as received. Compound 7 was prepared according to a literature procedure.  $^{27}$ 

Instrumentation. Proton nuclear magnetic resonance spectra (<sup>1</sup>H NMR) were recorded on a Bruker NEO Nanobay 400 MHz spectrometer at 24 °C. Chemical shifts are expressed in parts per million (ppm,  $\delta$  scale) downfield from tetramethylsilane and are referenced to residual protium in the NMR solvent (CHCl<sub>3</sub>,  $\delta$  7.26; DMSO,  $\delta$  2.51). Data are represented as follows: chemical shift, multiplicity (s = singlet, d = doublet, t = triplet, q = quartet, m = multiplet and/or multiple resonances, br = broad, app = apparent), integration, and coupling constant in Hertz. Proton-decoupled carbon nuclear magnetic resonance spectra (13C NMR) were recorded on a Bruker NEO Nanobay spectrometer at 100 MHz at 24 °C. Chemical shifts are expressed in parts per million (ppm,  $\delta$  scale) downfield from tetramethylsilane and are referenced to the carbon resonances of the solvent (CDCl<sub>3</sub>,  $\delta$  77.16; DMSO- $d_6$ ,  $\delta$  39.51). Decoupled fluorine nuclear magnetic resonance spectra (19F NMR) were recorded on a Bruker NEO Nanobay spectrometer at 101 MHz at 24 °C. Chemical shifts are expressed in parts per million (ppm,  $\delta$  scale). All NMR data were processed using MestReNova 14.2.3 software. All IR spectra were measured with a Nicolet iS5 FT-IR spectrophotometer with ATR diamond. Data are represented with frequency of absorption in cm<sup>-1</sup>. High-resolution mass spectrometry (HRMS) data were acquired on an Agilent 6530 Q-TOF mass spectrometer in positive ESI and processed with Agilent MassHunter software at Brown University. UV-vis spectra were recorded on a Shimadzu UV-2600i spectrometer in 10 mm quartz cuvettes at 23 °C. Spectra were processed using LabSolutions 1.10 software. Emission spectra were recorded on a Horiba Scientific Fluoromax Plus in 10 mm quartz cuvettes at 23 °C. Spectra were processed using FluorEssence 3.9 software. All CD measurements were recorded on a Jasco J-1100 CD spectrometer under a constant flow of nitrogen at 23 °C and processed using Spectra Manager software at the University of Rhode Island. Melting points were taken on a Stanford Research Systems DigiMelt MPA160 melting point apparatus. VCD (with corresponding IR collected simultaneously) spectra were recorded on a BioTools ChiralIR 2X DualPEM FT-VCD at 4 cm<sup>-1</sup> resolution, with PEM maximum frequencies at  $1400~\text{cm}^{-1}$  in a  $100~\mu\text{m}$  BaF<sub>2</sub> SL4 heavy duty IR cell from International Crystal Laboratories.

Synthetic Procedures. Synthesis of N-(2,2-Dimethoxyethyl)-1methyl-1H-indole-2-carboxamide (4). 1-Methyl-1H-indole-2-carboxylic acid (5.0 g, 29 mmol, 1.0 equiv) was dissolved in dioxane (57 mL) in an oil bath at 60 °C in an oven- and flame-dried round-bottom flask equipped with a nitrogen balloon. Once dissolved, carbonyldiimidazole (CDI, 4.62 g, 28.5 mmol, 1.0 equiv) was added portionwise, and the mixture was purged with nitrogen for 10 min. 2,2-Dimethoxyethan-1-amine (3.73 mL, 34.2 mmol, 1.2 equiv) was added via a syringe, and the resulting mixture was purged with nitrogen for another 10 min. The mixture was then refluxed in an oil bath at 60 °C overnight under a nitrogen atmosphere. After cooling to room temperature, water was added dropwise until the reaction was quenched. Ethyl acetate (200 mL) was added, and the organic layer was washed with water (3  $\times$  100 mL). The combined aqueous layers were washed with ethyl acetate (1  $\times$  100 mL). The organic layers were combined and dried over anhydrous magnesium sulfate, filtered, and concentrated to yield a beige solid (7.31 g, 98%) that was used without further purification. Analytical data for 4 was consistent with reports from the literature.

Synthesis of 9-Methyl-9H-pyrido[3,4-b]indol-1-yl Trifluoromethanesulfonate (5). N-(2,2-Dimethoxyethyl)-1-methyl-1H-indole-2carboxamide (7.31 g, 27.9 mmol, 1.0 equiv) was dissolved in trifluoroacetic acid (28 mL) in an oven- and flame-dried roundbottom flask. The solution was stirred vigorously under a nitrogen atmosphere at room temperature overnight. The solution was diluted with methanol (55 mL), and the precipitate was collected by filtration and washed with water. The solid was transferred to a beaker and basified with K2CO3. The mixture was filtered and washed with water to provide a white solid (4.61 g, 83%) that was used without further purification. Analytical data for 5 was consistent with reports from the literature. 19 9-Methyl-2,9-dihydro-1*H*-pyrido[3,4-*b*]indol-1-one (106 mg, 0.50 mmol, 1.0 equiv) was dissolved in pyridine (5 mL) in an oven- and flame-dried round-bottom flask and cooled to 0 °C. Trifluoromethanesulfonic anhydride (171  $\mu$ L, 1.00 mmol, 2.0 equiv) was added dropwise over 1 min at 0 °C, and then the mixture was warmed to room temperature and stirred for 4 h. The product was diluted with water (50 mL) and extracted with ethyl acetate (3 × 50 mL). The organic layer was washed with 1 M hydrochloric acid (3 × 50 mL), dried over anhydrous magnesium sulfate, filtered, and concentrated on silica gel. The product was then purified via automated flash-column chromatography using ethyl acetate and hexanes, resulting in a white powder (171 mg, 96%).  $R_f = 0.52$  (10%) ethyl acetate-hexanes; UV), mp = 148-150 °C. ¹H NMR (400 MHz, CDCl<sub>3</sub>)  $\delta$  (ppm) 8.14 (ddd, J = 8.0, 1.2, 0.7 Hz, 1H), 8.10 (d, J = 5.1Hz, 1H), 8.00 (d, I = 5.2 Hz, 1H), 7.69 (ddd, I = 8.4, 7.1, 1.2 Hz, 1H), 7.53 (dt, J = 8.5, 0.8 Hz, 1H), 7.37 (ddd, J = 8.0, 7.1, 0.9 Hz, 1H), 4.13 (s, 3H).  $^{13}$ C{ $^{1}$ H} NMR (101 MHz, CDCl<sub>3</sub>)  $\delta$  (ppm) 142.6, 141.0, 135.5, 134.4, 129.6, 126.0, 121.9, 120.90, 120.88, 118.8 (q, *J* = 321.2 Hz), 116.0, 110.0, 31.7. <sup>19</sup>F NMR (376 MHz, CDCl<sub>3</sub>)  $\delta$  (ppm) -72.61. IR (FT-IR) cm<sup>-1</sup>: 2948, 1697, 1636, 1550, 1468, 1410, 1322, 1135, 1075, 925, 802, 763. HRMS (m/z):  $[M + H]^+$  calcd for C<sub>13</sub>H<sub>10</sub>F<sub>3</sub>N<sub>2</sub>O<sub>3</sub>S, 331.0364; found, 331.0371.

Synthesis of 9-Methyl-1-(2-methylnaphthalen-1-yl)-9H-pyrido-[3,4-b]indole (rac-1d). 9-Methyl-9H-pyrido[3,4-b]indol-1-yl trifluoromethanesulfonate (90 mg, 0.27 mmol, 1.0 equiv), (2-methylnaphthalen-1-yl)boronic acid (109 mg, 0.580 mmol, 2.0 equiv), tetrakis-(triphenylphosphine)palladium(0) (31 mg, 0.027 mmol, 0.1 equiv), and potassium carbonate (75 mg, 0.54 mmol, 2.0 equiv) were dissolved in a 95:5 mixture of dioxane (2.57 mL) and water (0.43 mL). The reaction mixture was stirred in a microwave tube and purged with nitrogen gas for 10 min and then heated in this sealed tube in the microwave at 130 °C for 30 min. The product mixture was diluted with ethyl acetate (50 mL) and washed with water (3 × 50 mL). The organic layer was dried over anhydrous sodium sulfate, filtered, and concentrated on silica gel. The product was then purified via automated flash-column chromatography using ethyl acetate and hexanes, resulting in a yellow solid (51.8 mg, 59%).  $R_f = 0.11$  (33%) ethyl acetate-hexanes; UV), mp = 73.4-75.6 °C. <sup>1</sup>H NMR (400 MHz,

CDCl<sub>3</sub>)  $\delta$  (ppm): 8.83 (t, J = 5.6 Hz, 1H), 8.51 (d, J = 6.1 Hz, 1H), 8.38 (dt, J = 8.0, 1.0 Hz, 1H), 8.06 (d, J = 8.8 Hz, 1H), 7.95 (dt, J = 8.6, 1.1 Hz, 1H), 7.82 (ddd, J = 8.4, 7.1, 1.2 Hz, 1H), 7.58 (d, J = 8.6 Hz, 1H), 7.53 (ddd, J = 8.0, 7.1, 0.8 Hz, 1H), 7.50–7.46 (m, 2H), 7.33 (ddd, J = 8.3, 6.9, 1.3 Hz, 1H), 6.89 (dq, J = 8.4, 0.9 Hz, 1H), 3.13 (s, 3H), 2.41 (s, 3H).  $^{13}$ C{ $^{1}$ H} NMR (101 MHz, DMSO- $^{1}$ d<sub>6</sub>)  $\delta$  (ppm): 141.9, 141.6, 138.5, 135.2, 134.7, 134.3, 132.7, 131.3, 128.6, 128.5, 128.43, 128.37, 128.04, 126.6, 125.2 (2C), 121.7, 120.4, 119.7, 114.1, 110.2, 30.0, 19.8. IR (FT-IR) cm<sup>-1</sup>: 3050, 2923, 2853, 1738, 1620, 1558, 1439, 1402, 1348, 1283, 1228, 1130, 1044, 813, 740. HRMS (m/z): [M + H]<sup>+</sup> calcd for C<sub>23</sub>H<sub>19</sub>N<sub>2</sub>, 323.1548; found, 323.1547.

Synthesis of 1-(2-Methoxynaphthalen-1-yl)-9-methyl-9H-pyrido-[3,4-b]indole (rac-1f). 9-Methyl-9H-pyrido[3,4-b]indol-1-yl trifluoromethanesulfonate (70 mg, 0.21 mmol, 1.0 equiv), (2-methoxynaphthalen-1-yl)boronic acid (85 mg, 0.42 mmol, 2.0 equiv), tetrakis-(triphenylphosphine)palladium(0) (23 mg, 0.021 mmol, 0.1 equiv), and potassium carbonate (58 mg, 0.42 mmol, 2.0 equiv) were dissolved in a 95:5 mixture of dioxane (2.0 mL) and water (0.1 mL). The reaction mixture was stirred in a microwave tube and purged with nitrogen gas for 10 min and then heated in this sealed tube in the microwave at 130  $^{\circ}\text{C}$  for 30 min. The product mixture was diluted with ethyl acetate (50 mL) and washed with water (3  $\times$  50 mL). The organic layer was dried over anhydrous sodium sulfate, filtered, and concentrated on silica gel. The product was then purified via automated flash-column chromatography using ethyl acetate and hexanes, resulting in a yellow solid (66.0 mg, 93%).  $R_f = 0.18$  (33%) ethyl acetate-hexanes; UV), mp = 120-123 °C. ¹H NMR (400 MHz, CDCl<sub>3</sub>)  $\delta$  (ppm) 8.66 (d, J = 5.4 Hz, 1H), 8.26 (dt, J = 7.9, 1.1 Hz, 1H), 8.17 (d, J = 5.4 Hz, 1H), 8.05 (dd, J = 9.2, 0.8 Hz, 1H), 7.89– 7.86 (m, 1H), 7.63 (ddd, J = 8.3, 7.1, 1.2 Hz, 1H), 7.44 (d, J = 9.1 Hz, 1.2 Hz1H), 7.38-7.32 (m, 3H), 7.31-7.27 (m, 1H), 7.09-7.05 (m, 1H), 3.85 (s, 3H), 3.22 (s, 3H).  $^{13}C\{^{1}H\}$  NMR (101 MHz, CDCl<sub>3</sub>)  $\delta$ (ppm) 155.5, 143.0, 138.1, 136.5, 136.2, 134.1, 131.6, 131.6, 130.7, 129.3, 128.8, 128.3, 127.5, 124.5, 124.1, 122.0, 120.8, 120.3, 114.3, 113.2, 109.8, 56.6, 30.42. IR (FT-IR) cm<sup>-1</sup>: 2936, 1621, 1592, 1456, 1439, 1330, 1264, 1252, 1147, 1064, 909, 810, 779, 657. HRMS (*m*/ z):  $[M + H]^+$  calcd for  $C_{28}H_{19}N_2O$ , 339.1497; found, 339.1493.

Chiral HPLC Resolution. The enantiomers of 1d, 1f, and 7 (10 mg/mL in EtOH) were separated on a Rigol 3000 HPLC system with a single-wavelength UV detector ( $\lambda$  = 254 nm). Sample injections of 25–50  $\mu$ L were separated on a Chiral Technologies Daicel IA (1d and 7) or IA-3 (1f) column with hexanes/isopropanol/diethylamine (96:4:0.5 and 80:20:0.5, respectively) as eluent. Data were analyzed and processed using Clarity 6.0 software. See the Supporting Information for full details and HPLC traces (Figures S1–S3).

Racemization Kinetics. Enantiomerically pure samples of 1d and 1f were incubated in DMSO in an oil bath at 135 °C, and aliquots were taken at various time intervals and injected onto a chiral HPLC column. The enantiomeric ratio was plotted as a function of time to

obtain a rate constant  $(k_{\text{obs}})$  using the equation:  $k_{\text{obs}} = \frac{\ln\left(\frac{1}{\%\text{ee}}\right)}{t}$ . The rate constant,  $k_{\text{obs}}$ , was then used to determine the experimental barrier to rotation  $(\Delta G_{\text{rot}})$  by substitution into the Eyring–Polanyi equation:  $\Delta G_{\text{rot}} = RT \ln\left(\frac{2Tk_{\text{b}}}{k_{\text{obs}}h}\right)$ , where  $k_{\text{b}}$  is the Boltzmann distribution constant and h is Planck's constant. The racemization kinetics experiments were performed in duplicate. See the Supporting Information for full details (Figures S4–S6 and Tables S1–S3).

**Ground-State and Transition-State Calculations.** 1-Aryl-β-carbolines 1a-j were assembled in GaussView 6.1.1, and the equilibrium geometry was optimized at the B3LYP/6-31G(d) level of theory in the gas phase at 298.15 K using Gaussian 16. A frequency calculation was performed to obtain the ground-state energy. The two transition states, resulting from the two coplanar orientations of the aryl rings, were determined by rotation about the  $C_{aryl}-C_{aryl}$  bond, followed by geometry optimization and frequency calculation using the QST3 function. Several iterations were needed to optimize the bond angles, bond lengths, and dihedrals. These calculations were also performed at the B3LYP/6-31G(d) level of theory in the gas phase. In

each case, the number of imaginary frequencies was 1. The calculated barrier to rotation ( $\Delta G_{\rm rot}$ , kcal/mol) was determined by subtracting the ground-state free energy from the lower of the two transition-state free energies.

**VCD Measurements.** A 5 mg sample of atropisomer (1d-entA, 1d-entB, 1f-entA, 1f-entB) was dissolved in 120  $\mu$ L of CDCl<sub>3</sub> and transferred to a BaF<sub>2</sub> IR cell with path length of 100  $\mu$ m. The instrumentation used for this experiment was a BioTools (Jupiter, Florida) ChiralIR 2X DualPEM FT-VCD, resolution 4 cm<sup>-1</sup>, PEM maximum frequency 1400 cm<sup>-1</sup>. The samples were measured for 6 blocks of 1 h each while being purged with dry air to remove water vapor. The IR spectra were processed by solvent subtraction and offset to zero at 2000 cm<sup>-1</sup>. The VCD blocks were averaged, then enantiomer-corrected  $\left(\frac{\text{Ent}_A - \text{Ent}_B}{2}\right)$  to produce the final spectra.

**VCD Calculations.** An attempted molecular mechanics search resulted in only one conformer for each compound 1d or 1f. Each structure (*R*-configuration for d and *S*-configuration for 1f) was minimized, and the frequencies were calculated using four different DFT methods (6-31G(d)/B3LYP, 6-31G(d)/B3PW91, cc-pVTZ/B3LYP, cc-pVTZ/B3PW91) using Gaussian '09. In each case, the CPCM (chloroform) solvent method was used. The resulting IR and VCD spectra were *x*-axis-scaled and plotted with a line width of 5 cm<sup>-1</sup> for comparison to the experimental spectra. The best results were achieved with the combination of cc-PVTZ/B3PW91 in both cases.

**ECD Calculations.** The optimized structures taken from the VCD calculations at the 6-31G(d)/B3LYP level were used to calculate the UV/ECD spectra at the same level using the time-dependent method. A total of 500 excited states were calculated, which was more than necessary to capture the UV/ECD spectra down to the experimental cutoff of  $\sim\!200$  nm. The results were *x*-axis-scaled and plotted at peak half-width at half-height of 0.333 eV for comparison to the experimental spectra.

#### ASSOCIATED CONTENT

#### Supporting Information

The Supporting Information is available free of charge at https://pubs.acs.org/doi/10.1021/acs.joc.2c01675.

<sup>1</sup>H and <sup>13</sup>C NMR of all new compounds, HPLC traces, racemization kinetics data, quantum yield measurements, ECD and VCD data, and computational data (PDF)

#### AUTHOR INFORMATION

#### **Corresponding Author**

Seann P. Mulcahy — Providence College, Providence, Rhode Island 02918, United States; orcid.org/0000-0003-4444-5119; Email: smulcahy@providence.edu

### **Authors**

Kristen M. Baker – Providence College, Providence, Rhode Island 02918, United States

Colby J. Agostino – Providence College, Providence, Rhode Island 02918, United States

Emily A. Orloff – Providence College, Providence, Rhode Island 02918, United States

Lorenzo D. Battistoni – Providence College, Providence, Rhode Island 02918, United States

Riley R. Hughes – Providence College, Providence, Rhode Island 02918, United States; orcid.org/0000-0002-5924-7775

Erin M. McHugh – Providence College, Providence, Rhode Island 02918, United States

Michael P. Shaw – Providence College, Providence, Rhode Island 02918, United States

Jordan Nafie – BioTools, Inc., Jupiter, Florida 33478, United States

Complete contact information is available at: https://pubs.acs.org/10.1021/acs.joc.2c01675

#### Notes

The authors declare no competing financial interest.

#### ACKNOWLEDGMENTS

S.P.M. gratefully acknowledges support for this research from the National Science Foundation Research in Undergraduate Institutions (1955132) and Major Research Instrumentation (1919644) programs. This work was also supported in part by a postdoctoral fellowship to K.M.B. from the Rhode Island Institutional Development Award Network of Biomedical Research Excellence from the National Institute of General Medical Sciences of the National Institutes of Health under Grant P20GM103430. The authors also thank M. Xian at Brown University for performing the HRMS measurements, the Brown University Center for Computation and Visualization for the use of their servers, and J. J. Breen at Providence College for help with the photophysical measurements.

#### REFERENCES

- (1) Kuhn, R.Molekulare Asymmetrie. In *Stereochemie*; Freudenberb, K., Ed.; Franz Deuticke: Leipzig, 1933; pp 803–824.
- (2) (a) Eliel, E. L.; Wilen, S.; Mander, L. N. Stereochemistry of Organic Compounds; Wiley Interscience: New York, 1994; pp 1119–1190. (b) Ōki, M.Recent Advances in Atropisomerism. In Topics in Stereochemistry; Allinger, N. L.; Eliel, E. L.; Wilen, S. H., Eds.; Wiley: Hoboken, NJ, 1983; Vol. 14, pp 1–81.
- (3) (a) Atropisomerism and Axial Chirality; Lassaletta, J. M., Ed.; World Scientific Publishing Company, 2019; p 676. (b) Da, B.-C.; Tan, B.Application for Axially Chiral Ligands. In Axially Chiral Compounds; Tan, B., Ed.; Wiley-VCH: Weinheim, Germany, 2021; pp 245–274.
- (4) (a) Adams, R.; Yuan, H. C. The Stereochemistry of Diphenyls and Analogous Compounds. *Chem. Rev.* 1933, 12, 261. (b) Bott, G.; Field, L. D.; Sternhell, S. Steric effects. A study of a rationally designed system. *J. Am. Chem. Soc.* 1980, 102, 5618. (c) Grein, F. Twist Angles and Rotational Energy Barriers of Biphenyl and Substituted Biphenyls. *J. Phys. Chem. A* 2002, 106, 3823–3827. (d) Meca, L.; Reha, D.; Havlas, Z. Racemization Barriers of 1,1'-Binaphthyl and 1,1'-Binaphthalene-2,2'-diol: A DFT Study. *J. Org. Chem.* 2003, 68, 5677–5680. (e) Leroux, F. Atropisomerism, Biphenyls, and Fluorine: A Comparison of Rotational Barriers and Twist Angles. *Chem-BioChem* 2004, 5, 644–649. (f) Mazzanti, A.; Lunazzi, L.; Minzoni, M.; Anderson, J. E. Rotation in Biphenyls with a Single Ortho-Substituent. *J. Org. Chem.* 2006, 71, 5474–5481.
- (5) Selected reviews: (a) Kumarasamy, E.; Raghunathan, R.; Sibi, M. P.; Sivaguru, J. Nonbiaryl and Heterobiaryl Atropisomers: Molecular Templates with Promise for Atropselective Chemical Transformations. *Chem. Rev.* **2015**, *115*, 11239–11300. (b) Zilate, B.; Castgrogiovanni, A.; Sparr, C. Catalyst-Controlled Stereoselective Synthesis of Atropisomers. *ACS Catal.* **2018**, 8, 2981–2988. (c) Cheng, J. K.; Xiang, S.-H.; Li, S.; Ye, L.; Tan, B. Recent Advances in Catalytic Asymmetric Construction of Atropisomers. *Chem. Rev.* **2021**, *121*, 4805–4902. (d) Carmona, J. A.; Rodriguez-Franco, C.; Fernandez, R.; Hornillos, V.; Lassaletta, J. M. Atropselective transformation of axially chiral (hetero)biaryls. From desymmetrization to modern resolution strategies. *Chem. Soc. Rev.* **2021**, *50*, 2968–2983.
- (6) (a) Tang, W.; Zhang, X. New Chiral Phosphorus Ligands for Enantioselective Hydrogenation. *Chem. Rev.* **2003**, *103*, 3029–3069. (b) Akiyama, T.; Itoh, J.; Fuchibe, K. Recent Progress in Chiral Brønsted Acid Catalysis. *Adv. Synth. Catal.* **2006**, *348*, 999–1010.

- (c) Brandes, S.; Niess, B.; Bella, M.; Prieto, A.; Overgaard, J.; Jørgensen, K. A. Non-Biaryl Atropisomers in Organocatalysis. Chem. -Eur. J. 2006, 12, 6039-6052. (d) Li, Y.-M.; Kwong, F.-Y.; Yu, W.-Y.; Chan, A. S. C. Recent Advances in Developing New Axially Chiral Phosphine Ligands for Asymmetric Catalysis. Coord. Chem. Rev. 2007, 251, 2119-2144. (e) Parmar, D.; Sugiono, E.; Raja, S.; Rueping, M. Complete Field Guide to Asymmetric BINOL-Phosphate Derived Bronsted Acid and Metal Catalysis: History and Classification by Mode of Activation, Bronsted Acidity, Hydrogen Bonding, Ion Pairing, and Metal Phosphates. Chem. Rev. 2014, 114, 9047-9153. (f) Wang, Y.-B.; Tan, B. Construction of Axially Chiral Compounds via Asymmetric Organocatalysis. Acc. Chem. Res. 2018, 51, 534-547. (7) Selected reviews: (a) McCormick, M. H.; Stark, W. M.; Pittenger, G. E.; Pittenger, R. C.; McGuire, J. M. Vancomycin, a New Antibiotic. I. Chemical and Biologic Properties. Antibiot. Annu. 1955, 3, 606-611. (b) Bringmann, G.; Mortimer, A. J. P.; Keller, P. K.; Gresser, M. J.; Garner, J.; Matthias, B. Atropselective synthesis of axially chiral biaryl natural compounds. Angew. Chem., Int. Ed. 2005, 44, 5384-5427. (c) Kozlowski, M. C.; Morgan, B. J.; Linton, E. C. Total Synthesis of Chiral Biaryl Natural Products by Asymmetric Biaryl Coupling. Chem. Soc. Rev. 2009, 38, 3193-3207. (d) Bringmann, G.; Gulder, T.; Gulder, T. A.; Breuning, M. Atroposelective total synthesis of axially chiral biaryl natural products. Chem. Rev. 2011, 111, 563-639. (e) Smyth, J. E.; Butler, N. M.; Keller, P. A. A twist of nature - the significance of atropisomers in biological systems. Nat. Prod. Rep. 2015, 32, 1562-1583.
- (8) Selected articles: (a) Wu, Y.-L.; Ferroni, F.; Pieraccini, S.; Schweizer, W. B.; Frank, B. B.; Spada, G. P.; Diederich, F. 1,2-Di(phenylethynyl)ethenes with Axially Chiral, 2,2'-Bridged 1,1'-Binapnthyl Substituents: Potent Cholesteric Liquid Crystal Inducers. Org. Biomol. Chem. 2012, 10, 8016–8026. (b) Wen, K.; Yu, S.; Huang, Z.; Chen, L.; Xiao, M.; Yu, X.; Pu, L. Rational Design of a Fluorescent Sensor to Simultaneously Determine Both the Enantiomeric Composition and Concentration of Chiral Functional Amines. J. Am. Chem. Soc. 2015, 137, 4517–4524. (c) Collins, B. S. L.; Kistemaker, J. C. M.; Otten, E.; Feringa, B. L. A Chemically Powered Unidirectional Rotary Molecular Motor Based on a Palladium Redox Cycle. Nat. Chem. 2016, 8, 860–866. (d) Zhu, Y.-Y.; Wu, X.-D.; Gu, S.-X.; Pu, L. Free Amino Acid Recognition: A Bisbinaphthyl-Based Fluorescent Probe with High Enantioselectivity. J. Am. Chem. Soc. 2019, 141, 175–181.
- (9) (a) Ahmed, A.; Bragg, R. A.; Clayden, J.; Lai, L. W.; McCarthy, C.; Pink, J. H.; Westlund, N.; Yasin, S. A. Barriers to rotation about the chiral axis of tertiary aromatic amides. Tetrahedron 1998, 54, 13277-13294. (b) Clayden, J.; Moran, W. J.; Edwards, P. J.; LaPlante, S. R. The challenge of atropisomerism in drug discovery. Angew. Chem., Int. Ed. 2009, 48, 6398-6401. (c) LaPlante, S. R.; Edwards, P. J.; Fader, L. D.; Jakalian, A.; Hucke, O. Revealing atropisomer axial chirality in drug discovery. ChemMedChem 2011, 6, 505-513. (d) LaPlante, S. R.; Fader, L. D.; Fandrick, K. R.; Fandrick, D. R.; Hucke, O.; Kemper, R.; Miller, S. P. F.; Edwards, P. J. Assessing atropisomer axial chirality in drug discovery and development. J. Med. Chem. 2011, 54, 7005-7022. (e) Zask, A.; Murphy, J.; Ellestad, G. A. Biological stereoselectivity of atropisomeric natural products and drugs. Chirality 2013, 25, 265-274. (f) Glunz, P. W. Recent encounters with atropisomerism in drug discovery. Bioorg. Med. Chem. Lett. 2018, 28, 53-60. (g) Toenjes, S. T.; Gustafson, J. L. Atropisomerism in medicinal chemistry: challenges and opportunities. Future Med. Chem. 2018, 10, 409-422.
- (10) (a) Kyba, E. P.; Gokel, G. W.; de Jong, F.; Koga, K.; Sousa, L. R.; Siegel, M. G.; Kaplan, L.; Sogah, D. Y.; Cram, D. J. Host-Guest Complexation. 7. The Binaphthyl Structural Unit in Host Compounds. J. Org. Chem. 1977, 42, 4173–4184. (b) Tkachenko, N. V.; Scheiner, S. Optical Stability of 1,1'-Binaphthyl Derivatives. ACS Omega 2019, 4, 6044–6049.
- (11) Tucker, S. C.; Brown, J. M.; Oakes, J.; Thornthwaite, D. Resolution and coupling of 1-(2'-hydroxy-1'naphthyl)isoquinolines. *Tetrahedron* **2001**, *57*, 2545–2554.

- (12) (a) Quinonero, O.; Jean, M.; Vanthuyne, N.; Roussel, C.; Bonne, D.; Constantieux, T.; Bressy, C.; Bugaut, X.; Rodriguez, J. Combining Organocatalysis with Central-to-Axial Chirality Conversion: Atroposelective Hantzsch-Type Synthesis of 4-Arylpyridines. Angew. Chem., Int. Ed. 2016, 55, 1401–1405. (b) Kashima, K.; Teraoka, K.; Uekusa, H.; Shibata, Y.; Tanaka, K. Rhodium-Catalyzed Atroposelective [2+2+2] Cycloaddition of Ortho-Substituted Phenyl Diynes with Nitriles: Effect of Ortho Substituents on Regio- and Enantioselectivity. Org. Lett. 2016, 18, 2170–2173. (c) Shao, Y.-D.; Dong, M.-M.; Wang, Y.-A.; Cheng, P.-M.; Wang, T.; Cheng, D.-J. Organocatalytic Atroposelective Friedlander Quinoline Heteroannulation. Org. Lett. 2019, 21, 4831–4836. (d) Wan, J.; Liu, H.; Lan, Y.; Li, X.; Hu, X.; Li, J.; Xiao, H.-P.; Jiang, J. Catalytic Asymmetric Synthesis of Atropisomeric Quinolines through the Friedlander Reaction. Synlett 2019, 30, 2198–2202.
- (13) (a) Ros, A.; Estepa, B.; Ramírez-López, P.; Álvarez, E.; Fernández, R.; Lassaletta, J. M. Dynamic Kinetic Cross-Coupling Strategy for the Asymmetric Synthesis of Axially Chiral Heterobiaryls. J. Am. Chem. Soc. 2013, 135, 15730-15733. (b) Bhat, V.; Wang, S.; Stoltz, B. M.; Virgil, S. C. Asymmetric Synthesis of QUINAP via Dynamic Kinetic Resolution. J. Am. Chem. Soc. 2013, 135, 16829-16832. (c) Staniland, S.; Adams, R. W.; McDouall, J. J. W.; Maffucci, I.; Contini, A.; Grainger, D. M.; Turner, N. J.; Clayden, J. Biocatalytic Dynamic Kinetic Resolution for the Synthesis of Atropisomeric Biaryl N-Oxide Lewis Base Catalysts. Angew. Chem., Int. Ed. 2016, 55, 10755-10759. (d) Hornillos, V.; Carmona, J. A.; Ros, A.; Iglesias-Sigüenza, J.; López-Serrano, J.; Fernández, R.; Lassaletta, J. M. Dynamic Kinetic Resolution of Heterobiaryl Ketones by Zinc-Catalyzed Asymmetric Hydrosilylation. Angew. Chem., Int. Ed. 2018, 57, 3777-3781. (e) Han, S. J.; Bhat, V.; Stoltz, B. M.; Virgil, S. C. Atroposelective Synthesis of PINAP via Dynamic Kinetic Asymmetric Transformation. Adv. Synth. Catal. 2019, 361, 441-444. (f) Zhang, L.; She, L.; Wu, S.; Zhong, G.; Wang, Y.; Tan, B. Design and Atroposelective Construction of IAN analogues by Organocatalytic Asymmetric Heteroannulation of Alkynes. Angew. Chem., Int. Ed. 2020, 59, 23077-23082. (g) Wang, Q.; Zhang, W.; Song, H.; Wang, J.; Zheng, C.; Gu, Q.; You, S. Rhodium-Catalyzed Atroposelective Oxidative C-H/C-H Cross-Coupling Reaction of 1-Aryl Isoquinoline Derivatives with Electron-Rich Heteroarenes. J. Am. Chem. Soc. 2020, 142, 15678-15685.
- (14) Cao, R.; Peng, W.; Wang, Z.; Xu, A. beta-Carboline alkaloids: biochemical and pharmacological functions. *Curr. Med. Chem.* **2007**, 14, 479–500.
- (15) (a) Badre, A.; Boulanger, A.; Abou-Mansour, E.; Banaigs, B.; Combaut, G.; Francisco, C. Eudistomin U and isoeudistomin U, new alkaloids from the Caribbean ascidian Lissoclinum fragile. J. Nat. Prod. 1994, 57, 528-533. (b) Kobayashi, J.; Harbour, G. C.; Gilmore, J.; Rinehart, K. L., Jr. Eudistomins A, D, G, H, I, J, M, N, O, P, and Q, bromo, hydroxy, pyrrolyl and iminoazepino .beta.-carbolines from the antiviral Caribbean tunicate Eudistoma olivaceum. J. Am. Chem. Soc. 1984, 106, 1526-1528. (c) Tulyaganov, T. S. Alkaloids from Nitraria komarovii. Structures of nitraridine, dihydronitraridine, and tetrahydronitraridine. Chem. Nat. Compd. 2006, 42, 459-461. (d) Tulyaganov, T. S.; Ibragimov, A. A.; Yunusov, S. Y.; Vakhabov, A. A.; Aminov, S. D.; Sultanov, M. B. Nitraria komarovii alkaloids. VII. Synthesis and pharmacological properties of nitramarin alkaloid. Khim.-Farm. Zh. 1984, 18, 1474-1476. (e) Yan, W.; Ge, H. M.; Wang, G.; Jiang, N.; Mei, Y. N.; Jiang, R.; Li, S. J.; Chen, C. J.; Jiao, R. H.; Xu, Q.; Ng, S. W.; Tan, R. X. Pictet-Spengler reaction-based biosynthetic machinery in fungi. Proc. Natl. Acad. Sci. U.S.A. 2014, 111, 18138-18143. (f) Shi, Y.; Xu, Z.; Tan, R.; Lei, X. Divergent Total Synthesis of Chaetoglines C to F. J. Org. Chem. 2019, 84, 8766-8770.
- (16) (a) Roggero, C. M.; Giulietti, J. M.; Mulcahy, S. P. Efficient synthesis of eudistomin U and evaluation of its cytotoxicity. *Bioorg. Med. Chem. Lett.* **2014**, 24, 3549–3551. (b) Giulietti, J. M.; Tate, P. M.; Cai, M.; Cho, B.; Mulcahy, S. P. DNA-binding studies of the natural  $\beta$ -carboline eudistomin U. *Bioorg. Med. Chem. Lett.* **2016**, 26, 4705–4708.

- (17) Selected references: (a) LaPlante, S. R.; Forgione, P.; Boucher, C.; Coulombe, R.; Gillard, J.; Hucke, O.; Jakalian, A.; Joly, M.-A.; Kukolj, G.; Lemke, C.; McCollum, R.; Titolo, S.; Beaulieu, P. L.; Stammers, T. Enantiomeric atropisomers inhibit HCV polymerase and/or HIV matrix: characterizing hindered bond rotations and target selectivity. J. Med. Chem. 2014, 57, 1944-1951. (b) Smith, D. E.; Marquez, I.; Lokensgard, M. E.; Rheingold, A. L.; Hecht, D. A.; Gustafson, J. L. Exploiting atropisomerism to increase the target selectivity of kinase inhibitors. Angew. Chem., Int. Ed. 2015, 54, 11754-11759. (c) Wang, J.; Zeng, W.; Li, S.; Shen, L.; Gu, Z.; Zhang, Y.; Li, J.; Chen, S.; Jia, X. Discovery and assessment of atropisomers of (±)-lesinurad. ACS Med. Chem. Lett. 2017, 8, 299-303. (d) Watterson, S. H.; Liu, Q.; Beaudoin Bertrand, M.; Batt, D. G.; Li, L.; Pattoli, M. A.; Skala, S.; Cheng, L.; Obermeier, M. T.; Moore, R.; Yang, Z.; Vickery, R.; Elzinga, P. A.; Discenza, L.; D'Arienzo, C.; Gillooly, K. M.; Taylor, T. L.; Pulicicchio, C.; Zhang, Y.; Heimrich, E.; McIntyre, K. W.; Ruan, Q.; Westhouse, R. A.; Catlett, I. M.; Zheng, N.; Chaudhry, C.; Dai, J.; Galella, M. A.; Tebben, A. J.; Pokross, M.; Li, J.; Zhao, R.; Smith, D.; Rampulla, R.; Allentoff, A.; Wallace, M. A.; Mathur, A.; Salter-Cid, L.; Macor, J. E.; Carter, P. H.; Fura, A.; Burke, J. R.; Tino, J. A. Discovery of Branebrutinib (BMS-986195): A strategy for identifying a highly potent and selective covalent inhibitor providing rapid in vivo inactivation of Bruton's tyrosine kinase (BTK). J. Med. Chem. 2019, 62, 3228-3250.
- (18) Bott, G.; Field, L. D.; Sternhell, S. Steric effects. A study of a rationally designed system. *J. Am. Chem. Soc.* **1980**, *102*, 5618–5626. (19) Barker, M. D.; Woodward, P. R.; Lewis, J. R. $\beta$ -Carboline herbicides and fungicides. GB215S462A, 1985.
- (20) Webb, N. J.; Marsden, S. P.; Raw, S. A. Rhodium(III)-Catalyzed C-H Activation/Annulation with Vinyl Esters as an Acetylene Equivalent. *Org. Lett.* **2014**, *16*, 4718–4721.
- (21) Barrett, K. T.; Miller, S. J. Regioselective derivatizations of a tribrominated atropisomeric benzamide scaffold. *Org. Lett.* **2015**, *17*, 580–583
- (22) Pardo, A.; Reyman, D.; Poyato, J. M. L.; Medina, F. Some  $\beta$ -carboline derivatives as fluorescence standards. *J. Lumin.* **1992**, *51*, 269–274.
- (23) (a) Snatzke, G. Circular Dichroism and Absolute Conformation: Application of Qualitative MO Theory to Chiroptical Phenomena. *Angew. Chem., Int. Ed.* **1979**, *18*, 363–377. (b) Berova, N.; DiBari, L.; Pescitelli, G. Application of electronic circular dichroism in configurational and conformational analysis of organic compounds. *Chem. Soc. Rev.* **2007**, *36*, 914–931. (c) Pescitelli, G.; Bruhn, T. Good Computational Practice in the Assignment of Absolute Configurations by TDDFT Calculations of ECD Spectra. *Chirality* **2016**, *28*, 466–474.
- (24) (a) He, Y.; Wang, B.; Dukor, R. K.; Nafie, L. A. Determination of Absolute Configuration of Chiral Molecules Using Vibrational Optical Activity: A Review. *Appl. Spectrosc.* **2011**, *65*, 699–723. (b) Merten, C.; Golub, T. P.; Kreienborg, N. M. Absolute Configurations of Synthetic Molecular Scaffolds from Vibrational CD Spectroscopy. *J. Org. Chem.* **2019**, *84*, 8797–8814. (c) Polavarapu, P. L.; Santoro, E. Vibrational optical activity for structural characterization of natural products. *Nat. Prod. Rep.* **2020**, *37*, 1661–1699. (d) Bogaerts, J.; Aerts, R.; Vermeyen, T.; Johannessen, C.; Herrebout, W.; Batista, J. M., Jr. Tackling Stereochemistry in Drug Molecules with Vibrational Optical Activity. *Pharmaceuticals* **2021**, *14*, 877.
- (25) (a) Freedman, T. B.; Cao, X.; Nafie, L. A.; Kalbermatter, M.; Linden, A.; Rippert, A. J. An Unexpected Atropisomerically Stable 1,1-Biphenyl at Ambient Temperature in Solution, Elucidated by Vibrational Circular Dichroism (VCD). *Helv. Chim. Acta* **2003**, *86*, 3141–3155. (b) Freedman, T. B.; Cao, X.; Nafie, L. A.; Kalbermatter, M.; Linden, A.; Rippert, A. J. Determination of the Atropisomeric Stability and Solution Conformation of Asymmetrically Substituted Biphenyls by Means of Vibrational Circular Dichroism (VCD). *Helv. Chim. Acta* **2005**, *88*, 2302–2314. (c) Pivonka, D. E.; Wesolowski, S. S. Vibrational Circular Dichroism (VCD) Chiral Assignment of Atropisomers: Application to γ-Aminobutyric Acid (GABA) Modu-

ı

lators Designed as Potential Anxiolytic Drugs. Appl. Spectrosc. 2013, 67, 365–371.

- (26) (a) Debie, E.; DeGussem, E.; Dukor, R. K.; Herrebout, W.; Nafie, L. A.; Bultinck, P. A Confidence Level Algorithm for the Determination of Absolute Configuration Using Vibrational Circular Dichroism or Raman Optical Activity. *ChemPhysChem* **2011**, *12*, 1542–1549. (b) Polavarapu, P. L.; Covington, C. L. Comparison of Experimental and Calculated Chiroptical Spectra for Chiral Molecular Structure Determination. *Chirality* **2014**, *26*, 539–552.
- (27) Foley, C. A.; Al-Issa, Y. A.; Hiller, K. P.; Mulcahy, S. P. Synthesis and Structure-Activity Relationships of 1-Aryl- $\beta$ -carbolines as Affinity Probes for the 5-Hydroxytryptamine Receptor. *ACS Omega* **2019**, *4*, 9807–9812.